Lattice dynamics of tetragonal $PbTiO_3$

Izumi Tomeno*
Faculty of Education and Human Studies, Akita University, Akita 010-8502, Japan

Yoshinobu Ishii
Neutron Science Research Center, Japan Atomic Energy Research Institute, Tokai, Ibaraki 319-0011, Japan

Yorihiko Tsunoda
Department of Applied Physics, School of Science and Engineering, Waseda University, Shinjuku, Tokyo 169-8555, Japan

Kunihiko Oka
Nanoelectronics Research Institute, National Institute of Advanced Industrial Science and Technology, Tsukuba, Ibaraki 305-8568, Japan
(Received 19 August 2005; revised manuscript received 11 January 2006; published 28 February 2006)

The phonon dispersion relations for tetragonal $PbTiO_3$ have been determined along the [100], [110], and [001] directions at room temperature by inelastic neutron scattering. The zone-boundary TA phonon energies for $PbTiO_3$ are considerably lower than those for $BaTiO_3$ and $SrTiO_3$, indicating the dominant role of Pb atoms in TA phonons. The zone-center TO-A_1 phonon energy is higher than the zone-center TO-E phonon energy. A preliminary high-temperature experiment has revealed the gradual softening of the TO-A_1 phonons and the stability of TO-E phonons up to 643 K (0.84 T_c). The TO-A_1 phonons have an extremely broad linewidth, in marked contrast to the well-defined TO-E phonons. The TO phonons at the zone-boundary M point indicate that the energy for the rotational mode of the oxygen octahedra is approximately half of that for the distortion of the octahedra along the c axis. The X-point TO phonon energies for $PbTiO_3$ are much higher than those for $Pb(Zn_{1/3}Nb_{2/3})O_3$, suggesting that the B-site atoms in ABO_3 contribute largely to the TO phonons in Pb-based perovskites. Present phonon dispersion relations are generally in agreement with the first-principles calculations for the zone-center and zone-boundary phonon energies.

DOI: 10.1103/PhysRevB.73.064116 PACS number(s): 77.80.−e, 77.84.−s, 63.20.−e

I. INTRODUCTION

Lead titanate $PbTiO_3$ and barium titanate $BaTiO_3$ occupy an important position in the family of perovskite ABO_3 compounds from both scientific and technological viewpoints. Lead titanate $PbTiO_3$ undergoes only a single first-order transition at T_c=763 K from a cubic paraelectric (PE) to a tetragonal ferroelectric (FE) phase. In contrast, $BaTiO_3$ exhibits FE phase transitions from the cubic PE to a succession of tetragonal, orthorhombic, and finally rhombohedral phases. Cohen[1] interpreted the distinctive behavior on the basis of first-principles calculations as follows. The covalent nature of Pb 6s and O 2p states is responsible for the stability of tetragonal $PbTiO_3$, whereas the ionic character of Ba and O atoms is essential to the existence of rhombodedral $BaTiO_3$.[1,2] Kuroiwa *et al.*[3] presented evidence for Pb-O covalency in tetragonal $PbTiO_3$ with a maximum-entropy method analysis on the synchrotron-radiation powder data.

In the 1970s, Shirane *et al.*[4] investigated the lattice dynamics of $PbTiO_3$ using the inelastic neutron scattering technique. The pioneer work has revealed the existence of a well-defined soft mode in cubic $PbTiO_3$. This contrasts strikingly with the overdamped soft mode in $BaTiO_3$.[5,6]Unfortunately, only a limited number of branches for $PbTiO_3$ were determined, partly because the crystal size was small.[4]

Lead titanate $PbTiO_3$ is also the end member of relaxor ferroelectrics $(1-x)Pb(Zn_{1/3}Nb_{2/3})O_3-xPbTiO_3$ (PZN-PT) and $(1-x)Pb(Mg_{1/3}Nb_{2/3})O_3-xPbTiO_3$ (PMN-PT).[7–9] The introduction of approximately 10% $PbTiO_3$ is crucial to the extraordinary huge piezoelectric and dielectric constants in the PZN-PT system.[9] Phonon dispersion relations have been studied extensively for relaxors such as PZN,[10,11] PMN,[12–14] PZN-PT,[15–17] and PMN-PT.[18] The low-lying TO phonon branch in these relaxors is found to drop sharply near the zone center. The long-wavelength TO phonons appear to couple with the corresponding TA phonons in relaxors.

The recent advance in first-principles methods made it possible to calculate the phonon dispersion relations in cubic and tetragonal $PbTiO_3$ at the symmetry positions of the Brillouin zone.[19–21] García and Vanderbilt[19] computed the phonon energies for tetragonal $PbTiO_3$ at the zone center and zone boundaries. Ghosez *et al.*[20] calculated the full phonon dispersion relations for cubic $PbTiO_3$ and cubic $BaTiO_3$. Experimental phonon data for $PbTiO_3$, however, do not permit a detailed comparison with first-principles lattice dynamics calculations for $PbTiO_3$.

In this paper, we present the phonon dispersion relations in tetragonal $PbTiO_3$ obtained by inelastic-neutron- scattering techniques. The data are compared with the first-principles calculations reported by García and Vanderbilt.[19] Furthermore, the lattice dynamics of $PbTiO_3$ is discussed in relation to those for the Pb-based relaxor PZN (Ref. 10) and the simple perovskite compounds $BaTiO_3$,[22] $SrTiO_3$,[23] $KTaO_3$,[24] and $KNbO_3$.[25]

II. EXPERIMENT

The inelastic-neutron-scattering experiments were performed on the triple-axis spectrometer TAS-1 installed at

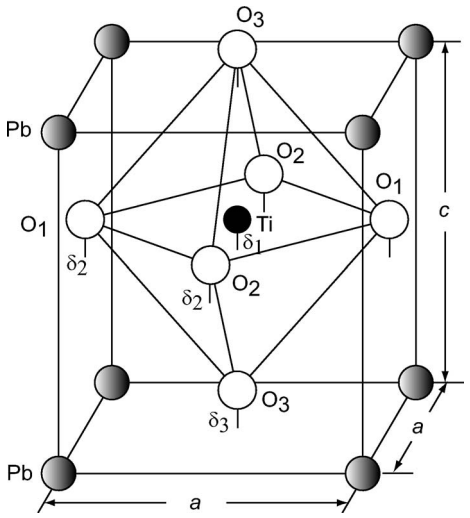

FIG. 1. Crystal structure of tetragonal $PbTiO_3$. Room-temperature values for lattice parameters a and c and positional parameters δ_i are given in Ref. 27.

JRR-3M, Tokai. Constant-**Q** scans were employed with neutron energy gain and fixed incident neutron energies (E_i) of 14.7, 30.5, and 42 meV. Constant-E scans were also made when necessary. Pyrolytic graphite (PG) crystals were used as monochromator and analyzer. A PG filter was placed before the sample to remove higher-order contamination. Collimations of 40′-40′-40′-40′ were adopted.

The single crystal used in this study was grown by the top-seeded solution growth method from a PbO flux. Details of the crystal growth have been reported in Ref. 26. The single crystal has a disk shape with a volume of approximately 5 cm^3. The crystal structure of tetragonal $PbTiO_3$ is illustrated in Fig. 1. The large spontaneous strain appears in the FE phase. The room-temperature lattice parameters measured by neutron diffraction are $a=3.900$ Å and $c=4.148$ Å, in agreement with the values reported in Ref. 27. The atomic positions are expressed in reduced coordinates as follows: Pb at (0,0,0), Ti at $(0.5,0.5,0.5+\delta_1)$, O_1 at $(0.5,0,0.5+\delta_2)$, O_2 at $(0,0.5,0.5+\delta_2)$, and O_3 at $(0.5,0.5,\delta_3)$, where the positional parameter δ_i represents the shift from the symmetrical position along the [001] direction.[27] Neutron diffraction shows that the most part of the sample has a single grain with the c axis oriented perpendicular to the disk. No electric field has been applied during cooling the sample. Thus a multiple FE domain may exist in the single-grain part of the sample; the spontaneous polarization is directed to the [001] or $[00\bar{1}]$ axis.

The Brillouin zone for tetragonal $PbTiO_3$ is shown in Fig. 2. There are 12 optic modes at the Γ point in $PbTiO_3$. The low-lying phonon dispersion curves were determined systematically at room temperature. In addition, a preliminary high-temperature experiment was carried out up to 693 K ($0.91T_c$). Acoustic and low-lying optic phonon data were collected along the $[\xi 00]$ (Δ), $[00\zeta]$ (Λ), and $[\xi\xi 0]$ (Σ) high-symmetry directions. The normal modes for tetragonal ABO_3 have been analyzed in Refs. 19, 25, and 28. Here we labeled the phonon branches in tetragonal $PbTiO_3$ with irreducible representations on the basis of the group-theoretical analysis

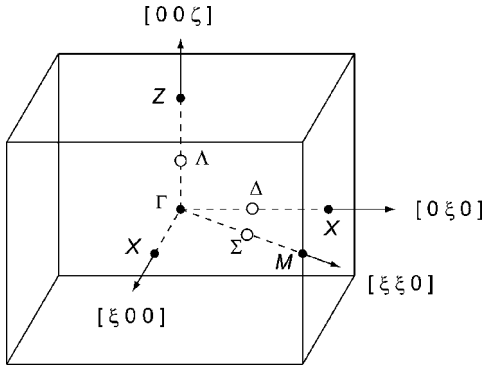

FIG. 2. Brillouin zone for tetragonal $PbTiO_3$. Data were collected along the Δ, Λ, and Σ high-symmetry directions.

performed by Fontana *et al.*[25] In addition, we assigned the zone-center and zone-boundary phonons by reference to the sequence of phonon frequencies for irreducible representations computed by García and Vanderbilt.[19] The Λ_1 branches represent purely longitudinal (L) modes, whereas the Δ_2 and doubly degenerate Λ_5 branches are purely transverse (T) modes. Except for the Λ_1, Δ_2, and Λ_5 branches, the polarization vectors have components along more than one high-symmetry direction. The Σ_1 and Δ_1 branches are longitudinal-like or transverse-like modes, and the Σ_2 branches are transverse-like modes.

III. PHONON DISPERSION RELATIONS

Figure 3 displays typical constant-**Q** scans for the TA-like and TO phonons at the zone-boundary M point. The phonon line shapes were fitted with the solid curves using a single or double Gaussian and a linear background. The instrumental energy resolution was typically 0.8 meV full width at half maximum (FWHM). Figure 4 shows the phonon dispersion curves for tetragonal $PbTiO_3$ measured at room temperature. The solid circles represent the phonon peak position, and the bars denote FWHM for the phonon peak. No corrections for

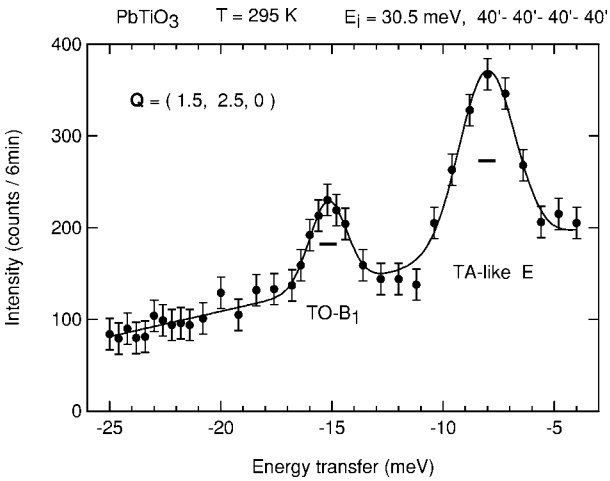

FIG. 3. Constant-**Q** scans for TA-like E and TO-B_1 phonons at the M point in $PbTiO_3$. The solid line is Gaussian fits to the data. The horizontal bars show the instrumental energy resolutions.

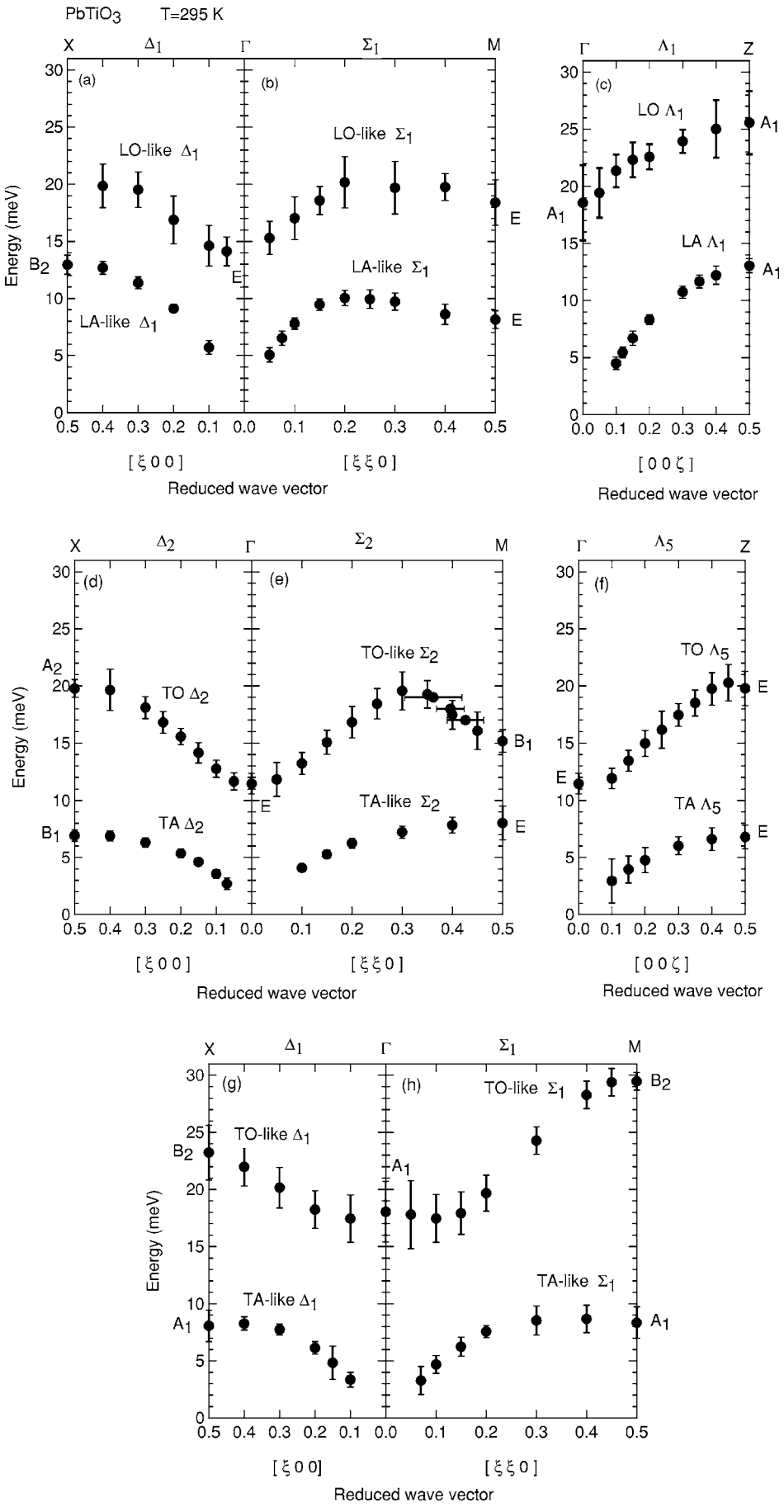

FIG. 4. Phonon dispersion curves for tetragonal $PbTiO_3$ measured at room temperature. Each solid circle and the attached bar refer to the phonon peak and its FWHM, respectively.

TABLE I. Zone-boundary acoustic phonon energies in tetragonal $PbTiO_3$. Normal-mode analysis and calculated phonon energies are taken from Ref. 19.

			Phonon energy (meV)	
Point	Mode	Basis	Present work	Calculation
X	LA-like B_2	Pb_x, Ti_z, O_{1x}, O_{1z}, O_{3z}	13.0±0.1	12.3
X	TA-like A_1	Pb_z, Ti_x, O_{1z}, O_{2z}, O_{3x}	8.1±0.2	8.2
X	TA B_1	Pb_y, O_{1y}	6.93±0.04	6.7
Z	LA A_1	Pb_z, Ti_z, $O_{1z}+O_{2z}$, O_{3z}	12.2±0.2	12.6
Z	TA E	Pb_x, Ti_x, O_{1x}, O_{2x}, O_{3x}	6.80±0.05	5.7
M	LA-like E	Pb_x, Ti_y, O_{2z}, O_{3y}	8.15±0.03	7.1
		Pb_y, Ti_x, O_{1z}, O_{3x}		
M	TA-like A_1	Pb_z, $O_{1y}+O_{2x}$	8.34±0.05	9.1
M	TA-like E	Pb_x, Ti_y, O_{2z}, O_{3y}	8.0±0.1	7.1
		Pb_y, Ti_x, O_{1z}, O_{3x}		

the instrumental resolution were made to the FWHM value for the phonon peak. Shirane *at al*.[4] have reported the phonon dispersion relations for the Δ_1 and Λ_5 branches in tetragonal $PbTiO_3$. The data obtained through this work are in good agreement with the dispersion curves reported earlier.

A. Acoustic modes

In this study, we determined five TA phonon dispersion relations in tetragonal $PbTiO_3$: Δ_1, Δ_2, Σ_1, Σ_2, and Λ_5 modes. The zone-boundary acoustic phonon energies are given in Table I. The TA phonons at the X, Z, and M points have a narrow energy range from 6.8 to 8.3 meV. This suggests the flat TA phonon dispersion relations along the zone boundaries, although the measurements have not been performed in the presnet study. Furthermore, the dispersion curve for the LA-like Δ_1 mode is almost the same as that for the LA-Λ_1 mode. As shown in Table I, the zone-boundary acoustic phonon energies determined by this study are in good agreement with those computed by García and Vanderbilt.[19]

The TA-phonon dispersion relations for $PbTiO_3$ are compared in Fig. 5 with those for tetragonal $BaTiO_3$,[22] cubic $SrTiO_3$,[23] cubic $KTaO_3$,[24] tetragonal $KNbO_3$,[25] and cubic PZN.[10] The zone-boundary TA phonon energies for tetragonal $PbTiO_3$ are considerably lower than those for tetragonal $BaTiO_3$ and cubic $SrTiO_3$. For $PbTiO_3$, $BaTiO_3$, and $SrTiO_3$, the TA phonon energies at the X point of the Δ_2 branches are roughly equal to those at the M point of the Σ_2 branches. The zone-boundary TA phonon energies for $PbTiO_3$ are also lower than those for $KNbO_3$ and $KTaO_3$, except for the X point. For $KTaO_3$ and $KNbO_3$, the M-point TA phonon energy is considerably higher than the X-point TA phonon energy.

To date, first-principles studies of full phonon dispersion relations for perovskite oxides have been concentrated on cubic perovskites.[20,29–31] Ghosez *et al.*[20,29] found a good correspondence between the calculated and experimental acoustic phonon energies for cubic $BaTiO_3$. First-principles calculations for cubic $BaTiO_3$ and cubic $PbTiO_3$ indicate that the TA phonons at the X and M points are mainly governed by the A (Pb or Ba) atom vibrations. Here we assume that the mode assignment of low-lying phonons is common in tetragonal $PbTiO_3$ and tetragonal $BaTiO_3$. In the tetragonal phase, the zone-boundary acoustic phonons at the X, M, and Z points involve the A atom displacements against the neighboring oxygen atoms.[19] The Ti atom in the tetragonal phase is at rest for the TA-B_1 mode at the X point and the TA-like A_1 mode at the M point. The Ti atom participates in the other zone-boundary acoustic modes. Figure 6 shows the TA phonon energies at X and M points against the inverse of square root of the A atom mass for ABO_3. A rough estimate suggests that zone-boundary TA phonon energies depend on the A atom mass, with the exception of the X-point TA phonon energies for $KNbO_3$ and $KTaO_3$. On the basis of a shell model for $KTaO_3$, Perry *et al.*[32] have explained the difference in TA phonon energies as follows. The low energy of X-point TA phonons is due to the dominant role of the B (Ta) atom oscillation, whereas the high energy of M-point TA phonons is governed by the A (K) atom oscillation.

The TA phonon energies for PZN and $PbTiO_3$ are lower than those for the other perovskites, as shown in Fig. 5. In

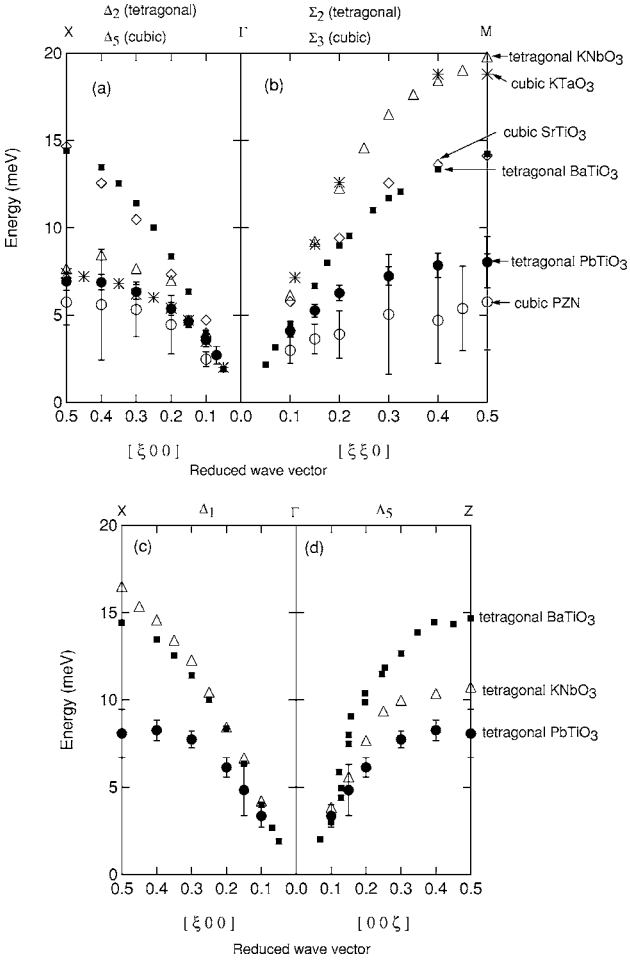

FIG. 5. TA phonon dispersion relations for typical perovskites. Results for $PbTiO_3$ are compared with those for tetragonal $BaTiO_3$ (Ref. 22), tetragonal $KNbO_3$ (Ref. 25), cubic $SrTiO_3$ (Ref. 23), $KTaO_3$ (Ref. 24), and cubic PZN (Ref. 10).

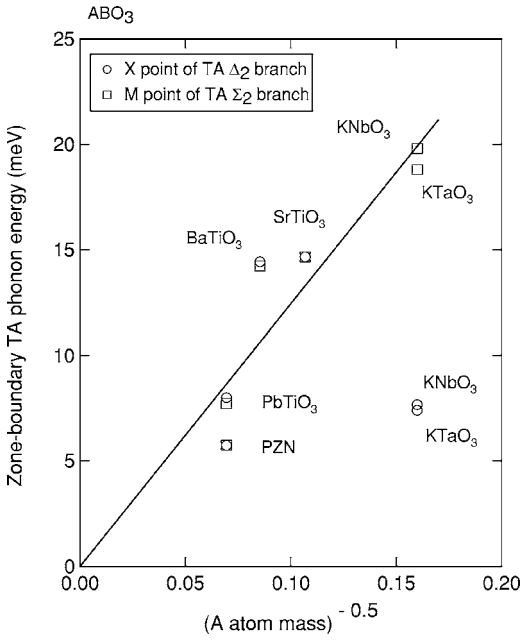

FIG. 6. TA phonon energies at the X and M points for ABO_3 as a function of the inverse of square root of the A atom mass. The M point data are fitted to a line. References to TA phonons for ABO_3 are the same as in Fig. 5.

Pb-based perovskites, the Pb atom vibration plays a major role in the TA phonon curves. In particular, the TA phonon energies for cubic PZN are lower than those for tetragonal $PbTiO_3$. A possible explanation is that the force constants for PZN are weaker than those for $PbTiO_3$. The TA phonon linewidths for $PbTiO_3$ are narrow in the entire zone, whereas those for PZN are extremely broad in the range $0.2 \leqslant \xi \leqslant 0.5$. The nominal charges at the B site are +2 on Zn and +5 on Nb in PZN. The charge neutrality fixes the atomic ratio of Zn to Nb as 1:2. Therefore, the microscopic polar regions, the distribution of B-site atom masses, and the strain fluctuations in PZN should contribute to the broadening of TA phonon linewidths.

The coupling of TA and TO phonon branches has been reported for tetragonal $BaTiO_3$ (Ref. 22) and tetragonal $KNbO_3$ (Ref. 25). Unlike tetragonal $BaTiO_3$, each TA phonon dispersion curve in $PbTiO_3$ displays normal behavior (Fig. 4). In particular, results for the Δ_2 and Λ_5 branches in $PbTiO_3$ indicate the absence of the TA and TO interaction at room temperature. We will treat this point in relation to the TO-E mode.

The elastic constants shown in Table II were derived from the slopes of each acoustic-phonon branch around $\mathbf{q}=0$. The elastic-constant values determined by this work are in good agreement with those taken from Brillouin-scattering experiments reported by Li *et al.*[33] The initial slope for the LA-Λ_1, TA-like Δ_1, and TA-like Σ_1 branches should give the elastic constants at constant polarization C_{33}^P, C_{44}^P, and C_{44}^P, respectively, on the condition that measurements are made for a single-FE-domain sample. We denote the corresponding elastic constants for the multidomain crystal by C_{ii}' ($i=3$ and 4). Elastic constants C_{33}^P and C_{44}^P in the tetragonal phase are given by

$$C_{33}^P = C_{33}^E + \frac{e_{33}^2}{\varepsilon_{33}^S}, \tag{1}$$

$$C_{44}^P = C_{44}^E + \frac{e_{15}^2}{\varepsilon_{11}^S}, \tag{2}$$

where C_{ii}^E is the elastic constant at constant field, e_{ij} is the piezoelectric constant, and ε_{ii}^S is the dielectric constant at constant strain. The second terms in Eqs. (1) and (2) represent the piezoelectric contributions. The distribution of FE domains may reduce the effective values for piezoelectric constants. Here we consider the two extreme cases for the effective elastic constant C_{33}' for the multi-FE-domain crystal. First, the average value of e_{33} is zero in the multidomain crystal. If the piezoelectric effect is canceled, C_{33}' for the multidomain crystal is equal to C_{33}^E. Second, the e_{33} value remains unchanged. Then C_{33}' is expected to be C_{33}^P. As in the C_{33}' case, we expect that C_{44}' for the multidomain crystal ranges from C_{44}^E to C_{44}^P. The Brillouin-scattering data for C_{33}^P, C_{44}^P, and C_{44}^E are shown in Table II. Li *et al.*[33] also estimated the value for C_{33}^E to be $(1.05 \pm 0.07) \times 10^{11}$ N/m^2. In view of these data, we interpret that C_{ii}' for the multidomain crystal is equal to C_{ii}^P ($i=3$ and 4). One possibility is that the FE domain size is significantly larger than the acoustic phonon wavelength determined by inelastic neutron scattering. The FE domains of large size may be produced by the spontane-

TABLE II. Acoustic modes and elastic constants for tetragonal $PbTiO_3$. Brillouin-scattering results are taken from Ref. 33.

Reduced wave vector	Mode	Elastic constant	Present work (10^{11} N/m^2)	Brillouin scattering (10^{11} N/m^2)
$[\xi 00]$	LA-like Δ_1	C_{11}^E	2.32±0.03	2.35±0.03
$[\xi 00]$	TA Δ_2	C_{66}^E	1.06±0.02	1.04±0.01
$[\xi 00]$	TA-like Δ_1	C_{44}^P	0.80±0.01	0.83±0.01
$[00\zeta]$	LA Λ_1	C_{33}^P	1.63±0.10	1.45±0.04
$[00\zeta]$	TA Λ_5	C_{44}^E	0.72±0.02	0.65±0.01
$[\xi\xi 0]$	LA-like Σ_1	$(C_{11}^E+C_{12}^E+2C_{66}^E)/2$	2.86±0.02	2.72±0.02
$[\xi\xi 0]$	TA-like Σ_1	C_{44}^P	0.83±0.02	0.83±0.01
$[\xi\xi 0]$	TA-like Σ_2	$(C_{11}^E-C_{12}^E)/2$	0.63±0.01	0.69±0.02

TABLE III. Zone-center optic phonon energies in tetragonal $PbTiO_3$. Raman-scattering data are taken from Ref. 34. Calculated phonon energies are taken form Ref. 19.

		Phonon energy (meV)		
Mode	Basis	Present work	Raman scattering	Calculation
TO E	Pb_x, Ti_x, O_{1x}, O_{2x}, O_{3x}	11.5±0.1	10.84	10.0
TO A_1	Pb_z, Ti_z, $O_{1z}+O_{2z}$, O_{3z}	18.1±0.1	18.41	18.7
LO E	Pb_x, Ti_x, O_{1x}, O_{2x}, O_{3x}		15.80	14.1
LO A_1	Pb_z, Ti_z, $O_{1z}+O_{2z}$, O_{3z}		24.05	23.2

ous strain. The remaining LA and TA branches near $\mathbf{q}=0$ give the elastic constants at constant field, C_{ij}^E, because the acoustic waves are free from the piezoelectric coupling. The initial slope for the TA-Λ_5 branch gives C_{44}^E, whereas those for the TA-like Δ_1 and Σ_1 branches give C_{44}^P. Table II shows that the present neutron-scattering experiment can distinguish between C_{44}^P and C_{44}^E.

Acoustic phonon energies computed by García and Vanderbilt[19] were confined to zone boundaries. Here we refer to first-principles calculations for elastic constants in cubic $PbTiO_3$ performed by Waghmare and Rabe.[21] The calculated lattice parameter[21] is approximately 2% less than the experimental data for the cubic phase. The calculated C_{ij} values using the experimental lattice parameter are as follows: $C_{11}=3.0\times10^{11}$ N/m^2, $C_{12}=1.3\times10^{11}$ N/m^2, and $C_{44}=3.5\times10^{11}$ N/m^2. Experimental results for C_{ij} in tetragonal $PbTiO_3$ suggest that first-principles calculations overestimate the elastic constant values for cubic $PbTiO_3$.

B. Optic modes

The zone-center and zone-boundary optic phonon energies are given in Tables III and IV, respectively. In view of Table I, III, and IV, acoustic and optic phonon energies determined by this study are generally in good agreement with the calculated phonon energies reported by García and Vanderbilt.[19]

Figure 4 shows that the energy of the zone-center TO-A_1 mode is significantly higher than that for the corresponding TO-E mode at room temperature. Raman-scattering experiments have been performed extensively to identify 12 optic modes in tetragonal $PbTiO_3$.[34–37] As shown in Table III, the zone-center TO phonon energies determined by this work are in good agreement with the Raman-scattering results.[34,35] However, the LO phonon dispersion curves shown in Fig. 4 seems inconsistent with the corresponding Raman results. We will discuss this point later. The Lyddane-Sacks-Teller (LST) relationship connects a complete set of the TO and LO phonon energies with the dielectric constants at constant strain, ε_{11}^S and ε_{33}^S. According to the dielectric-constant measurements,[33] the room-temperature value for $\varepsilon_{11}^S/\varepsilon_0$ is 101 and that for $\varepsilon_{33}^S/\varepsilon_0$ is 34. The dielectric-constant relation $\varepsilon_{11}^S>\varepsilon_{33}^S$ mainly corresponds to the fact that the low-lying zone-center TO-A_1 mode is well stiffened at room temperature.

The temperature dependence of the phonon dispersion curves is plotted in Fig. 7. The TO-like Σ_1 phonon branch is found to be temperature dependent in the limited $\mathbf{q}$ range up to $\mathbf{q}=[0.2,0.2,0]$. Figure 8 shows the zone-center TO phonon energy versus temperature. The TO-A_1 mode in the FE phase corresponds to the TO-F_{1u} mode in the PE phase. Shirane *et al.*[4] reported that the energy of the TO-F_{1u} mode is 3 meV at 783 K ($1.03T_c$). The energy of the zone-center TO-A_1 mode decreases to 12.7 meV with increasing temperature up to 643 K ($0.84T_c$), whereas that of the zone-center TO-E mode practically remains constant. The distinct temperature dependence of these TO modes is consistent with the Raman-scattering results reported by Fontana *et al.*[37] Constant-E

TABLE IV. Zone-boundary optic phonon energies in tetragonal $PbTiO_3$. Normal-mode analysis and calculated phonon energies are taken from Ref. 19.

			Phonon energy (meV)	
Point	Mode	Basis	Present work	Calculation
X	LO-like A_1	Pb_z, Ti_x, O_{1z}, O_{2z}, O_{3x}		29.4
X	TO-like B_2	Pb_x, Ti_z, O_{1x}, O_{2z}, O_{3z}	23.2±0.2	21.9
X	TO A_2	Ti_y, O_{2y}, O_{3y}	19.8±0.2	16.2
Z	LO A_1	Pb_z, Ti_z, $O_{1z}+O_{2z}$, O_{3z}	25.6±0.5	23.4
Z	TO E	Pb_x, Ti_x, O_{1x}, O_{2x}, O_{3x}	19.8±0.2	18.7
M	LO-like E	Pb_x, Ti_y, O_{2z}, O_{3y} Pb_y, Ti_x, O_{1z}, O_{3x}	18.4±0.5	25.2
M	TO-like B_2	Ti_z, $O_{1y}+O_{2x}$, O_{3z}	29.5±0.1	30.6
M	TO B_1	$O_{1y}-O_{2x}$	15.2±0.1	17.1

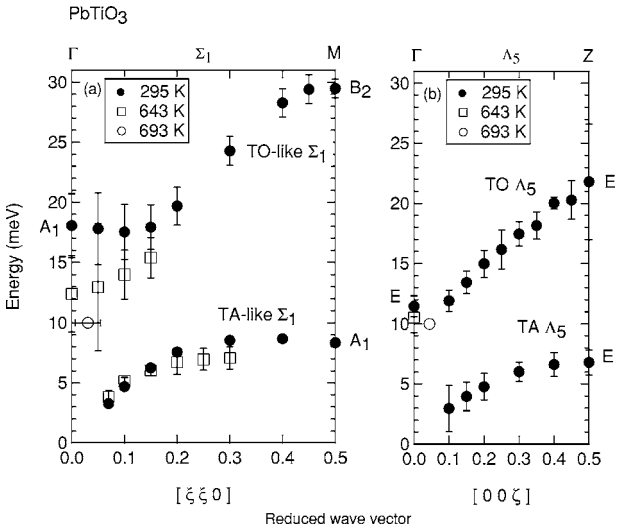

FIG. 7. Temperature dependence of phonon dispersion curves for tetragonal $PbTiO_3$.

scans around the Γ point show that the energies for the zone-center TO-A_1 and TO-E modes are approximately 10 meV at 693 K ($0.91T_c$). These results suggest a small difference between ε_{11} and ε_{33} at $0.91T_c$. In the FE phase ε_{33}^S increases gradually with increasing temperature and then shows an abrupt increase in the close vicinity of T_c.[38,39] In the PE phase ε_{33}^S should be equal to ε_{11}^S. Above T_c, ε is expressed by a Curie-Weiss law $\varepsilon = C/(T-T_0)$, where T_0 is the extrapolated Curie temperature. The difference $T_c - T_0$ is 43 K for $PbTiO_3$.[38] The temperature dependence of ε_{33}^S is characterized by a first-order phase transition.[38] According to the LST relationship, the distinctive behavior of the TO modes above and below T_c is closely connected with the temperature dependence of ε_{33}^S.

Figure 9 shows typical constant-**Q** scans for the small-**q** optic phonons. The TO-A_1 phonons have an extremely broad linewidth, whereas the TO-E phonons are well defined. In addition, the FWHM of the TO-like Σ_1 phonon peak for $\mathbf{q}=[0,0,0.05]$ is larger than that for the TO-like Σ_2 phonon peak. The linewidths of the observed phonon peaks are affected by the spectrometer resolution function and the slope of the dispersion curve. However, we can expect that the distinct linewidth difference remains unchanged after correcting the raw data, because no focusing effect is predicted at the Γ point with flat dispersion relations. The broad peak of the TO-like Σ_1 mode around $\mathbf{q}=0$ seems consistent with the Raman-scattering experiment for the TO-A_1 mode.[34,35] Foster *et al.*[34,35] interpreted the anomalous Raman spectrum in terms of an anharmonic nature of the lattice. The anharmonic effect appears to play an important role in the large tetragonal strain and the large polarization along the c axis in $PbTiO_3$. On the other hand, Cho *et al.*[40,41] reported that lattice defects also contribute to the lowest-energy Raman subpeak (13.7 meV) of the TO-A_1 mode. Figure 9 shows that the peak position for the TO-A_1 phonons deviates noticeably from the subpeak (−13.7 meV) related to lattice defects. Therefore the damping of the TO-A_1 mode mainly originates from the intrinsic feature of $PbTiO_3$.

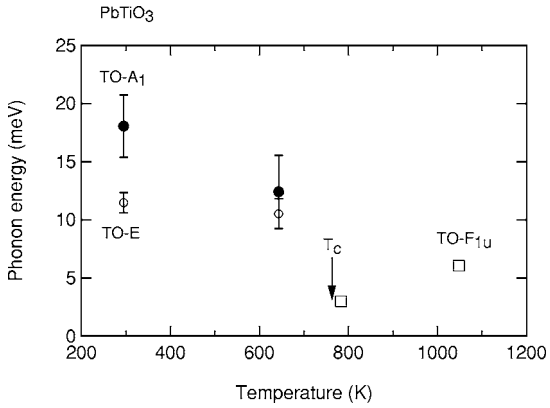

FIG. 8. Zone-center TO phonon energy vs temperature for $PbTiO_3$. The data above T_c are taken from Ref. 4.

The energy of TO-E phonons is weakly temperature dependent, as shown in Figs. 7 and 8. The Raman-scattering experiment[42] also shows that the frequency of the TO-E mode is nearly constant between 40 and 300 K. Therefore, both experimental results support the stability of tetragonal $PbTiO_3$. Figure 4 shows that the low-lying TO phonon energies for the Δ_2 and Λ_5 modes are widely separated from those for the corresponding TA phonons at room temperature. The TO-Δ_2 and TO-Λ_5 modes are well defined for tetragonal $PbTiO_3$. For tetragonal $BaTiO_3$, the TO-Δ_2 and TO-Λ_5 modes have low energies and cross over the corresponding TA modes.[22] The softening of the TO-E phonon mode in tetragonal $BaTiO_3$ and tetragonal $KNbO_3$ indicates the tendency toward a transition to the orthorhombic phase at low temperature.[22,25]

Kobayashi *et al.*[43,44] have reported that $PbTiO_3$ undergoes a phase transition to an orthorhombic phase at 183 K. García and Vanderbilt[19] showed that the reported low-temperature phase transition should be driven by the unstable zone-center B_1 optic mode where the O_1 and O_2 atoms move in opposite directions along the c axis. The calculated B_1 mode energy is 35.8 meV, significantly higher than the energy for the TO-E or TO-A_1 mode determined by this study. García and Vanderbilt[19] concluded that a simple transition due to the zone-center or zone-boundary instability is not likely in FE $PbTiO_3$ at low temperatures. Figure 4 also presents no evidence for an instability at 295 K.

Figure 10 plots a series of constant-**Q** scans for the LO-Λ_1 phonons along $[00\zeta]$ in conjunction with the zone-center LO phonon energies determined by Raman scattering.[34,35] It was impossible to distinguish the LO phonon from the TO phonon at the zone center. A possible explanation is that the intensity of the broad TO phonon peak at the zone center is dominant over that for the corresponding LO phonon peak. The scans at $\mathbf{Q}=(0,0,4+\zeta)$ in the range $0<\zeta<0.5$ should satisfy the longitudinal-mode configuration. However, the transverse optic phonons may be also included in the data, due to the finite resolution width. A series of scans for the LO-Λ_1 phonons strongly suggests that the energy for the LO-A_1 mode is lower than 24 meV, the energy determined by Raman scattering.[34,35] It has been reported that the Raman intensity for the LO-A_1 mode is also weak.[34,35] The situation is further complicated, because the LO-A_1 phonon energy

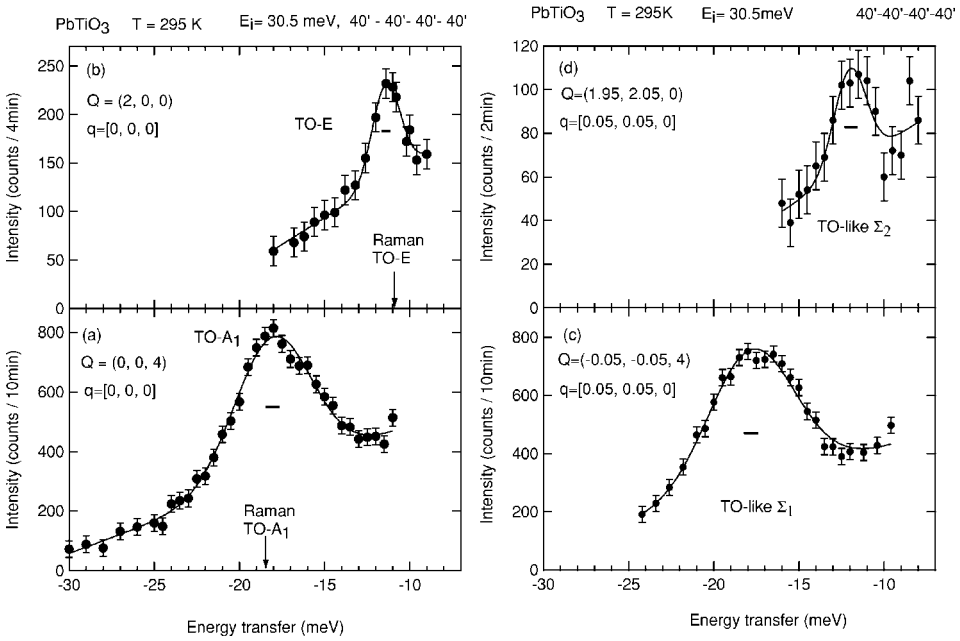

FIG. 9. Constant-**Q** scans for optic phonons for $\mathbf{q}=(\xi,\xi,0)$. The horizontal bars indicate the instrumental resolutions. The arrows represent the corresponding Raman data for TO-E and TO-A_1 phonons taken from Ref. 35.

determined by Raman scattering is in good agreement with the value calculated by García and Vanderbilt.[19]

Figure 4 shows that the TO-like Σ_2 phonon dispersion relation shows the maximum around $\mathbf{q}=[0.3,0.3,0]$ and then decreases toward the zone boundary. In contrast, the TO-like Σ_1 phonon curve increases monotonically with increasing $|\mathbf{q}|$. At the M point the energy of the TO-B_1 mode is approximately half of that for the TO-like B_2 mode. The TO-B_1 mode at the M point represents the rotational motion of the oxygen octahedra along the c axis, whereas the TO-like B_2 mode at the M point is associated with the distortion of oxygen octahedral and the Ti atom shift along the c axis.[19] Thus the stiffening of the TO-like B_2 mode reflects the rigidity of the oxygen octahedra.

First-principles calculations[20,21,45] for cubic $PbTiO_3$ indicate the coexistence of the most unstable zone-center FE mode and the weak unstable antiferrodistortive mode at the R point of the TO-Λ_3 branch. In addition, the TO-Σ_3 mode is unstable toward the M point.[20,21] In cubic perovskites, these zone-boundary TO modes represent the rotational motion of oxygen octahedra. The decrease in energy around the M point for the TO-like Σ_2 branch in the FE phase is related to the low energy of zone-boundary TO modes in the PE phase. In contrast, the oxygen rotational modes are stable in $BaTiO_3$ and $KNbO_3$.[20,29,31,45]

Relaxor PZN undergoes a structural phase transition from a low-temperature rhombohedral to a high-temperature cubic phase at $T_c=413$ K.[7,8] We have studied the lattice dynamics of cubic PZN at 423 K using the same spectrometer.[10] The TO phonon dispersion curves for PZN are compared in Fig. 11 with those for tetragonal $PbTiO_3$. For PZN the TO branches drop sharply with decreasing ξ. The absence of a well-defined TO phonon around the zone center is common with Pb-based relaxors.[10–18] Here, we are concerned with TO phonons in the range $0.1\leqslant\xi\leqslant0.5$. The TO-$\Delta_5$ phonon energies for cubic PZN are lower than the TO-Δ_2 and TO-like Δ_1 phonon energies for tetragonal $PbTiO_3$. Except for the M point, the TO-Σ_3 phonon energies for PZN are lower than the TO-like Σ_2 phonon energies for $PbTiO_3$. The X-point normal modes for TO-Δ_2 and TO-Δ_5 branches are expressed by the B atom displacement against the O_1 and O_2 atoms. The X-point TO-Δ_5 phonon energy for PZN is about 15% less

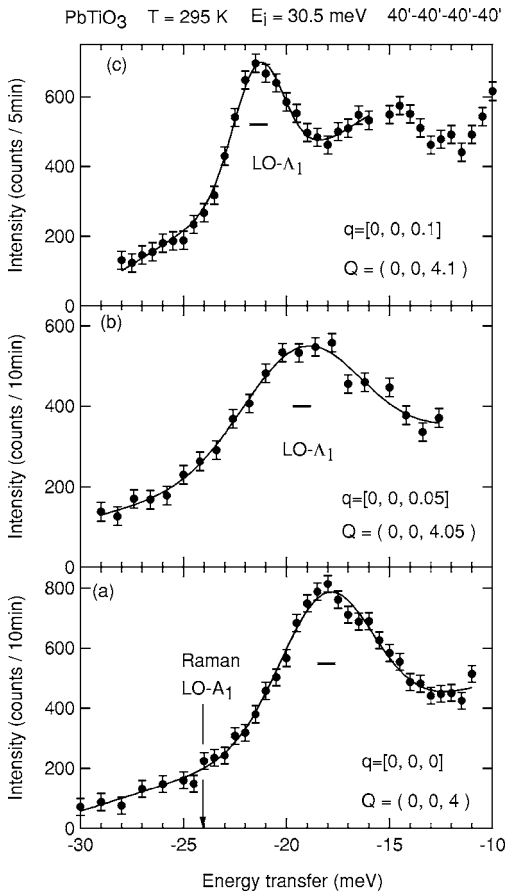

FIG. 10. Constant-**Q** scans for the LO-Λ_1 phonons. The horizontal bars indicate the instrumental resolutions. The arrow denotes the Raman data for the LO-A_1 phonons taken from Ref. 35.

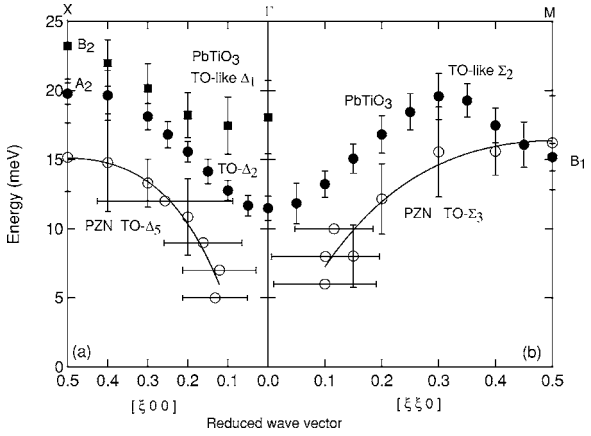

FIG. 11. TO phonon dispersion relations for tetragonal $PbTiO_3$ and cubic PZN. The PZN data are taken from Ref. 10.

than the X-point TO-Δ_2 phonon energy for $PbTiO_3$. The 15% decrease at the X point is roughly explained by the B atom mass contribution. Therefore, the B atoms play a major role in determining the TO phonon behavior in Pb-based perovskite oxides. The linewidths for the TO-Δ_5 mode in PZN are extremely broader than those for the TO-Δ_2 mode in $PbTiO_3$. There is a large difference in TA phonon linewidths between PZN and $PbTiO_3$, as previously mentioned.

IV. CONCLUSION

The lattice dynamics of tetragonal $PbTiO_3$ has been investigated along the $[\xi 00]$, $[\xi\xi 0]$, and $[00\zeta]$ directions at room temperature. The TA phonons at the X, Z, and M points exhibit a narrow energy range. The zone-boundary TA phonon energies for $PbTiO_3$ are approximately half of those for $BaTiO_3$ and $SrTiO_3$. The TA phonon energies for $PbTiO_3$ are slightly higher than those for PZN. Results for the TA phonons indicate that the Pb atom displacement plays a dominant role in the TA phonons.

The zone-center energy for the TO-A_1 mode is much higher than that for the TO-E mode. This corresponds to the dielectric constant relationship $\varepsilon_{11}^S > \varepsilon_{33}^S$ at room temperature. The TO-A_1 phonons have an extremely broad linewidth, in contrast to the well-defined TO-E phonons. A preliminary high-temperature experiment up to 643 K has revealed a close approach of the TO-A_1 phonon energy to the TO-E phonon energy. The TO-like phonons at the M point indicate that the energy for the rotation of the oxygen octahedra is approximately half of that for the distortion of the octahedra along the c axis. Except for the M point, the TO phonon energies for $PbTiO_3$ are higher than those for PZN. For Pb-based perovskites, B atom displacements play a major role in the TO phonons.

The phonon dispersion relations determined by this study are generally in good agreement with the first-principles calculations performed by García and Vanderbilt.[19] The stability of the TO phonons determined at 295 K seems inconsistent with the existence of a phase transition at 183 K reported by Kobayashi *et al.*[43,44]

ACKNOWLEDGMENTS

We would like to thank A. García for sending us a set of the mode eigenvectors for tetragonal $PbTiO_3$ not written explicitly in Ref. 19. We are also grateful to stimulating discussions with N. Wakabayashi, Y. Uesu, K. Kohn, H. Unoki, J. A. Fernandez-Baca, and J. L. Robertson.

*Electronic address: tomeno@gipc.akita-u.ac.jp

[1] R. E. Cohen, Nature (London) **358**, 136 (1992).
[2] R. E. Cohen and H. Krakauer, Phys. Rev. B **42**, 6416 (1990).
[3] Y. Kuroiwa, S. Aoyagi, A. Sawada, J. Harada, E. Nishibori, M. Takata, and M. Sakata, Phys. Rev. Lett. **87**, 217601 (2001).
[4] G. Shirane, J. D. Axe, J. Harada, and J. P. Remeika, Phys. Rev. B **2**, 155 (1970).
[5] Y. Yamada, G. Shirane, and A. Linz, Phys. Rev. **177**, 848 (1969).
[6] J. Harada, J. D. Axe, and G. Shirane, Phys. Rev. B **4**, 155 (1971).
[7] J. Kuwata, K. Uchino, and S. Nomura, Ferroelectrics **37**, 579 (1981).
[8] J. Kuwata, K. Uchino, and S. Nomura, Jpn. J. Appl. Phys., Part 1 **21**, 1298 (1982).
[9] S.-E. Park and T. R. Shrout, J. Appl. Phys. **82**, 1804 (1997).
[10] I. Tomeno, S. Shimanuki, Y. Tsunoda, and Y. Ishii, J. Phys. Soc. Jpn. **70**, 1444 (2001).
[11] P. M. Gehring, S.-E. Park, and G. Shirane, Phys. Rev. B **63**, 224109 (2001).
[12] P. M. Gehring, S. Wakimoto, Z.-G. Ye, and G. Shirane, Phys. Rev. Lett. **87**, 277601 (2001).
[13] S. Wakimoto, C. Stock, R. J. Birgeneau, Z.-G. Ye, W. Chen, W. J. L. Buyers, P. M. Gehring, and G. Shirane, Phys. Rev. B **65**, 172105 (2002).
[14] S. Wakimoto, C. Stock, Z.-G. Ye, W. Chen, P. M. Gehring, and G. Shirane, Phys. Rev. B **66**, 224102 (2002).
[15] P. M. Gehring, S.-E. Park, and G. Shirane, Phys. Rev. Lett. **84**, 5216 (2000).
[16] D. La-Orauttapong, B. Noheda, Z.-G. Ye, P. M. Gehring, J. Toulouse, D. E. Cox, and G. Shirane, Phys. Rev. B **65**, 144101 (2002).
[17] J. Hlinka, S. Kamba, J. Petzelt, J. Kulda, C. A. Randall, and S. J. Zhang, Phys. Rev. Lett. **91**, 107602 (2003).
[18] T. Y. Koo, P. M. Gehring, G. Shirane, V. Kiryukhin, S.-G. Lee, and S.-W. Cheong, Phys. Rev. B **65**, 144113 (2002).
[19] A. García and D. Vanderbilt, Phys. Rev. B **54**, 3817 (1996).
[20] P. Ghosez, E. Cockayne, U. V. Waghmare, and K. M. Rabe, Phys. Rev. B **60**, 836 (1999).
[21] U. V. Waghmare and K. M. Rabe, Phys. Rev. B **55**, 6161 (1997).
[22] G. Shirane, J. D. Axe, J. Harada, and A. Linz, Phys. Rev. B **2**, 3651 (1970).
[23] W. G. Stirling, J. Phys. C **5**, 2711 (1972).
[24] R. Comés and G. Shirane, Phys. Rev. B **5**, 1886 (1972).
[25] M. D. Fontana, G. Dolling, G. E. Kugel, and C. Carabatos, Phys. Rev. B **20**, 3850 (1979).
[26] K. Oka, H. Unoki, H. Yamaguchi, and H. Takahashi, J. Cryst. Growth **166**, 380 (1996).

[27] A. M. Glazer and S. A. Mabud, Acta Crystallogr., Sect. B: Struct. Crystallogr. Cryst. Chem. **34**, 1065 (1978).
[28] J. D. Freire and R. S. Katiyar, Phys. Rev. B **37**, 2074 (1988).
[29] P. Ghosez, X. Gonze, and J.-P. Michenaud, Ferroelectrics **206-207**, 205 (1998).
[30] C. Lasota, C.-Z. Wang, R. Yu, and H. Krakauer, Ferroelectrics **194**, 109 (1997).
[31] R. Yu and H. Krakauer, Phys. Rev. Lett. **74**, 4067 (1995).
[32] C. H. Perry, R. Currat, H. Buhay, R. M. Migoni, W. G. Stirling, and J. D. Axe, Phys. Rev. B **39**, 8666 (1989).
[33] Z. Li, M. Grimsditch, X. Xu, and S.-K. Chan, Ferroelectrics **141**, 313 (1993).
[34] C. M. Foster, M. Grimsditch, Z. Li, and V. G. Karpov, Phys. Rev. Lett. **71**, 1258 (1993a).
[35] C. M. Foster, Z. Li, M. Grimsditch, S.-K. Chan, and D. J. Lam, Phys. Rev. B **48**, 10160 (1993b).
[36] G. Burns and B. A. Scott, Phys. Rev. B **7**, 3088 (1973).
[37] M. D. Fontana, H. Idrissi, G. E. Kugel, and K. Wojcik, J. Phys.: Condens. Matter **3**, 8695 (1991).
[38] J. P. Remeika and A. M. Glass, Mater. Res. Bull. **5**, 37 (1970).
[39] Z. Li, M. Grimsditch, C. M. Foster, and S.-K. Chan, J. Phys. Chem. Solids **57**, 1433 (1996).
[40] S. M. Cho and H. M. Jang, Appl. Phys. Lett. **76**, 3014 (2000).
[41] S. M. Cho, H. M. Jang, and T.-Y. Kim, Phys. Rev. B **64**, 014103 (2001).
[42] D. Heiman and S. Ushioda, Phys. Rev. B **17**, 3616 (1978).
[43] J. Kobayashi, Y. Uesu, and Y. Sakemi, Phys. Rev. B **28**, 3866 (1983).
[44] J. Kobayashi and R. Ueda, Phys. Rev. **99**, 1900 (1955).
[45] W. Zhong and D. Vanderbilt, Phys. Rev. Lett. **74**, 2587 (1995).